JOURNAL OF SPACECRAFT AND ROCKETS
Vol. 43, No. 5, September–October 2006

Nozzle Plume Impingement on Spacecraft Surfaces: Effects of Surface Roughness

C. Ngalande,* T. Lilly,* M. Killingsworth,* and S. Gimelshein†
University of Southern California, Los Angeles, California 90089
and
A. Ketsdever‡
U.S. Air Force Research Laboratory, Edwards Air Force Base, California 93524

An experimental and numerical effort was undertaken to assess the effects of a cold-gas ($T_0 = 300$ K) nozzle plume impinging on simulated spacecraft surfaces. The nozzle flow impingement is investigated experimentally using a nanonewton resolution force balance and numerically using the direct simulation Monte Carlo numerical technique. The Reynolds number range investigated in this study is from approximately 2 to 350 using nitrogen propellant. The thrust produced by the nozzle was first assessed on a force balance to provide a baseline case. Subsequently, aluminum plates were attached to the same force balance parallel to the plume flow to simulate spacecraft surfaces in proximity to the thruster. Three plates were used, an electropolished plate with smooth surface and two rough surface plates with equally spaced rectangular and triangular grooves. A 15% degradation in thrust was observed both experimentally and numerically for the plate relative to the free plume expansion case. The effect of surface roughness on thrust was found to be small due to molecules backscattered from the plate to the nozzle plenum wall. Additionally, the influence of surface roughness in the diverging part of the nozzle on thrust was examined numerically and found to be significant at Reynolds numbers less than 10.

I. Introduction

WHEN in orbit, spacecraft require onboard or secondary propulsion systems to perform orbit transfer, orbit maintenance, and attitude control maneuvers. An important issue in the use of any spacecraft propulsion system involves the assessment and reduction of effects caused by the interaction between the thruster plume and spacecraft surfaces.[1] Direct impingement of a thruster plume on surfaces can generate unwanted torques, localized surface heating, and surface contamination. Self-impingement, that is, the impingement of a thruster plume on a host satellite surface, generally occurs for small surface angles with respect to the propulsion system's thrust vector or occurs in the thruster backflow. Cross impingement, that is, the impingement of one spacecraft's thruster plume onto another spacecraft, can occur at essentially any angle and is becoming increasingly important with the advent of microsatellite constellations. Many studies, both numerical[2–4] and experimental,[5,6] have been performed by various investigators to assess the impingement of plumes onto surfaces.

In recent years, micropropulsion systems have been developed to address the need for highly mobile microspacecraft. A wide array of concepts will require the expansion of propellant gases through microscale nozzles. Because many micropropulsion systems will also operate at relatively low pressures, the investigation of low-Reynolds-number flow has become increasingly important.[7] In the present study, an experimental and numerical effort has been developed to assess the effects of a nozzle plume impinging on a simulated spacecraft surface. Special attention is paid to the impact of roughness on surface forces and flowfield structure.

Received 3 August 2005; revision received 18 November 2005; accepted for publication 29 November 2005.

*Graduate Student, Department of Aerospace and Mechanical Engineering.
†Research Assistant Professor, Department of Aerospace and Mechanical Engineering.
‡Group Leader, Nonequilibrium Flows Group, Propulsion Directorate.

The nozzle flow impingement is investigated experimentally using a nanonewton resolution force balance and numerically using the direct simulation Monte Carlo (DSMC) method. The purpose of this work is to extend previous nozzle plume impingement results,[5,8] to the low-Reynolds-number-flow range for application to micropropulsion systems. The Reynolds number range investigated in this study is from 2 to approximately 350, based on the nozzle throat diameter using a molecular nitrogen propellant.

II. Experimental Setup

All thrust measurements were performed on the nanonewton thrust stand (nNTS), which has been described in detail by Jamison et al.[9] The nNTS was installed in chamber 4 of the Collaborative High Altitude Flow Facilities (CHAFF-4), which is a 3-m-diam, 6-m-long cylindrical, high vacuum chamber. The facility was pumped with a 1-m-diam diffusion pump with an alternate pumping speed of 25,000 l/s for molecular nitrogen. The ultimate facility pressure was approximately 10^{-4} Pa with all operational pressures below 10^{-2} Pa. A previous study[10] has shown that at these background pressures and corresponding thrust levels there is a negligible effect of background pressure on the thrust measurements in CHAFF-4.

The conical De Laval nozzle used in this study is shown schematically in Fig. 1. The conical nozzle was scaled from the geometry used by Rothe.[11] The scaled Rothe geometry has a 30-deg subsonic section, a relatively sharp 1-mm-diam throat with radius of curvature $r_c = d_t/4$, a 20-deg diverging section, and an expansion ratio of 62.4. This geometry was selected because there is extensive experimental data for it, which were previously used to verify the DSMC model's accuracy.[12,13] The nozzle machined from aluminum was attached to a cylindrical aluminum plenum and mounted on the nNTS. Figure 2 shows a scanning electron microscope image of the nozzle side wall, where the surface features caused by the machining process are clearly evident. The effect of the rough diverging section walls on the nozzle's performance parameters will be investigated numerically in subsequent sections.

After the free expansion thrust was measured, aluminum engineering surfaces with different surface roughness were attached to the thrust stand in the configuration shown in Fig. 1. The following three surfaces were used: 1) a electropolished flat surface (called smooth hereafter), 2) a surface with triangular (prismlike) grooves perpendicular to the plume axis, and 3) a surface with rectangular

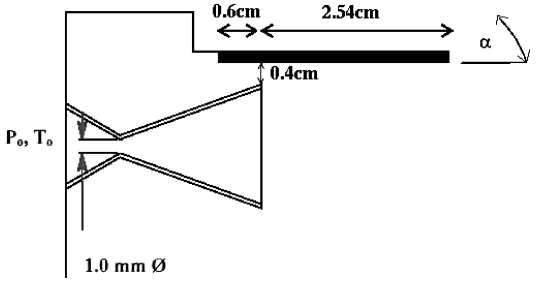

Fig. 1 Geometric setup in experiment.

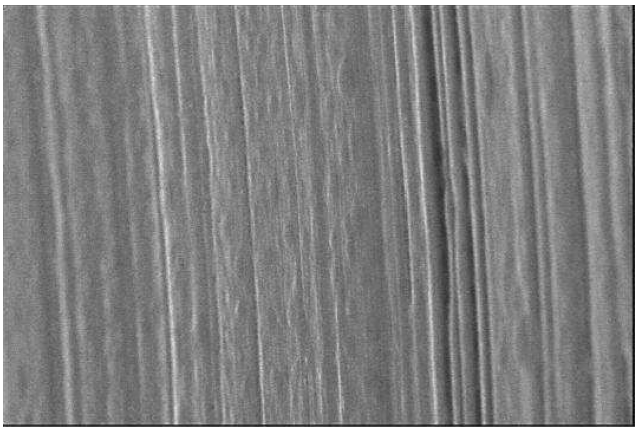

Fig. 2 Scanning electron microscope image, surface roughness of expanding section of conical nozzle.

grooves perpendicular to the plume axis. The grooves are equally spaced with a spacing of 0.05 cm. The angle of triangular grooves is 90 deg, and the depth of rectangular grooves is the same as their thickness of 0.05 cm. The length of the plate in the plume direction is 3 cm, and its width is 3.81 cm. The grooves are made only in the 2.45-cm-long region downstream from the nozzle exit plane.

The total force measured on the nNTS for this configuration is given by

$$F_{\text{tot}} = F_{\text{th}} - F_s + F_b \tag{1}$$

where F_{th} is the thrust produced by the nozzle in the absence of the plate, F_s is the incident shear force on the plate (acting in the opposite direction as the thrust force), and F_b is the force exerted on the plenum wall due to gas pressure in the backflow. The angle of the plate was varied from 0 to 10 deg. The surface temperature was 300 K.

The propellant was introduced to the plenum through an adjustable needle valve located downstream of a mass flow meter. In the experimental configuration, the mass flow meters were operated in the continuum regime throughout the pressure range investigated. The propellant used was molecular nitrogen. In this study, the stagnation pressures ranged from about 13 to approximately 2300 Pa, and the stagnation temperature was measured to be 300 K. The combination of stagnation pressure and temperature gave maximum Reynolds numbers of 350.

III. Numerical Method

Two geometric configurations have been considered in the computations. First, the free nozzle expansion into a vacuum has been modeled. The experimental nozzle geometry has been used with stagnation pressures ranging from 18 to 1800 Pa. Second, a three-dimensional interaction of the nozzle plume with a plate, smooth or rough, is simulated. The computational geometry includes the nozzle with the external side of the plenum and the plate, which size and location correspond to the experimental setup.

The DSMC-based software system SMILE[14] was used in all computations. The important features of SMILE that are relevant to this work are parallel capability, different collision and macroparameter grids with manual and automatic adaptations, and spatial weighting for axisymmetric flows. The majorant frequency scheme was used to calculate intermolecular interactions. The intermolecular potential was assumed to be variable hard sphere. Energy redistribution between the rotational and translational modes was performed in accordance with the Larsen–Borgnakke model. A temperature-dependent rotational relaxation number was used. The reflection of molecules on the surface was assumed to be diffuse with complete energy and accommodation.

All walls were assumed to be at a temperature of 300 K, except where specified otherwise, and the propellant gas was nitrogen at a stagnation temperature of 300 K. A background pressure of zero was set in all calculations. In the first series of computations (nozzle plume expansion into a vacuum), the computational domain included a part of the plenum large enough to avoid the impact of the domain size on the results, and the total number of collision cells and molecules was about 400,000 and 4,000,000, respectively. The three-dimensional plume–surface interaction was modeled using a starting surface at the nozzle exit, generated using an axisymmetric solution of a nozzle plume expansion. An elliptic distribution function was used for inflow molecules. The number of simulated molecules and cells was about 20,000,000 and 3,000,000, respectively.

IV. Nozzle Surface Roughness

A close examination of the surface structure inside the actual nozzle manifested a very rough, groovelike structure, as shown in Fig. 2, with micrometer-size grooves set out perpendicular to the main flow direction. The evident surface roughness prompted the authors to study numerically the effect of roughness inside the nozzle on thrust. To this end, axisymmetric DSMC computations were performed for a rough surface of the diverging part of the nozzle, assumed to have a regular triangular, saw-toothed structure with the triangle angle of 90 deg and the triangle base of 10 μm. The diffuse model of reflection with full energy and momentum accommodation was used on triangle surfaces. A total of more than 1000 was used, and the results are compared with those obtained for a flat diffusely reflecting surface (called smooth hereafter).

The comparison of number density fields inside a rough and a smooth nozzle is presented in Fig. 3 for the smallest chamber pressure considered, $P_0 = 18$ Pa. Note that the mean free path of the gas is over 500 times larger than the surface roughness size, and the flow may, therefore, be considered as free molecular based on this roughness size. Figure 3 also illustrates the geometry of the nozzle and the computational domain. The results show that the influence of the surface roughness in the diverging part propagates into the plenum and the density for the rough surface is about 10% higher than the corresponding values inside the smooth nozzle. This is explained by the fact that the flow is mostly subsonic in the nozzle and only becomes supersonic near the exit. The difference between rough and smooth is larger near the surface than at the centerline and amounts to almost 20% at the nozzle lip. The larger density for the rough case is explained by a significant amount of molecules,

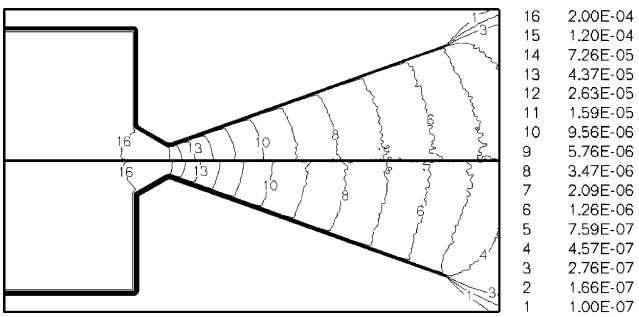

Fig. 3 Mass density fields for smooth (top) and rough (bottom) nozzles.

Table 1 Impact of surface roughness on nozzle properties

P_o, N/m^2	Surface type	Mass flow, kg/s	Thrust, N	I_{sp}, s
1.821×10^3	Smooth	0.2804×10^{-5}	0.1780×10^{-2}	0.6475×10^2
1.821×10^3	Rough	0.2800×10^{-5}	0.1770×10^{-2}	0.6449×10^2
1.821×10^2	Smooth	0.2301×10^{-6}	0.1176×10^{-3}	0.5213×10^2
1.821×10^2	Rough	0.2226×10^{-6}	0.1122×10^{-3}	0.5143×10^2
1.821×10^1	Smooth	0.1548×10^{-7}	0.7424×10^{-5}	0.4892×10^2
1.821×10^1	Rough	0.1375×10^{-7}	0.6614×10^{-5}	0.4908×10^2

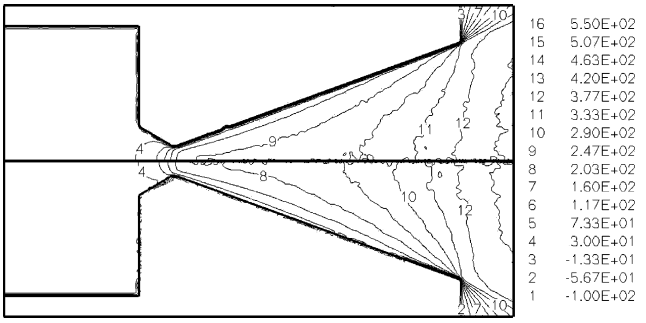

Fig. 4 Axial velocity fields for smooth (top) and rough (bottom) nozzles.

traveling toward the throat, that are reflected on the windside of the triangles.

The molecules reflected on the windside of triangles increase density and decrease axial velocity in the diverging part of the nozzle. This decrease in axial velocity, however, is compensated by the contribution from molecules reflected on the triangle lee sides that on average are reflected in the axial direction. The combined effect of these two trends results in a small influence of the surface roughness on the axial flow velocity fields, as shown in Fig. 4. Although there is a visible difference near the nozzle surface, with the rough case values at the surface being lower by over 50 m/s, the profiles at the nozzle exit are close.

The quantitative impact of the surface roughness inside the nozzle on the flow properties is given in Table 1, where the nozzle performance properties are shown for three plenum pressures. As expected, the effect of roughness is maximum at the lowest pressure, with the rough case mass flow being over 12% lower than the corresponding smooth case. Because the axial velocity at the nozzle exit is weakly affected by the surface roughness, the thrust force is also about 12% lower, and the specific impulse does not change with roughness. For a 10 times larger pressure, $P_0 = 180$ Pa, the surface roughness causes only a 3% decrease in the mass flow and practically no change in the specific impulse. At an even higher pressure of 1800 Pa, no visible influence of the nozzle roughness was found.

The conclusion from these computations is that the surface roughness in the nozzle impacts mostly the density fields; its effect on the axial velocity is much smaller. The mass flow is significantly reduced by the surface roughness only for throat-based Reynolds numbers of about unity or lower, when the subsonic region occupies large part of the diverging part of the nozzle. The surface roughness was found to have little effect on the specific impulse. This also shows that the experimental data on plume and surface forces shown in subsequent sections as a function of the mass flow rate are not affected by the nozzle surface roughness.

V. Interaction of Plume with a Plate: Numerical Modeling

Consider now the three-dimensional interaction of a rarefied plume with a plate. The pressure flowfield in the plane perpendicular to the plate surface and coming through the nozzle axis is given in Fig. 5 for a smooth plate and the stagnation pressure of 405 Pa. The interaction region between the plume and the plate is clearly seen, with the local pressure maximum located near the plate surface

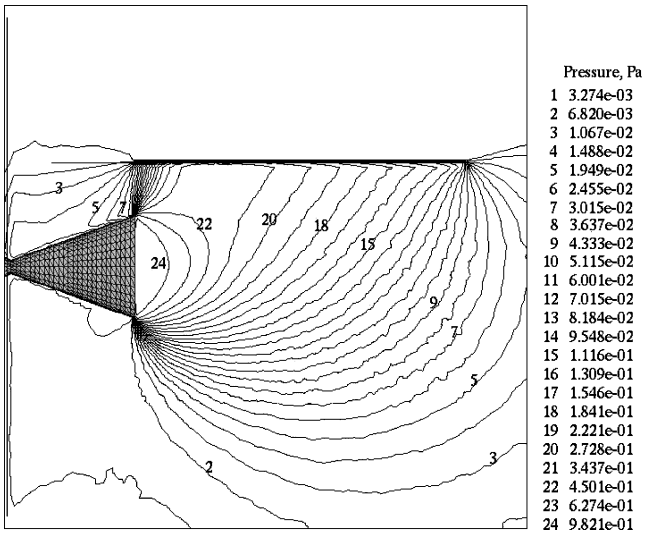

Fig. 5 Pressure field (pascals) over smooth plate at 0 deg.

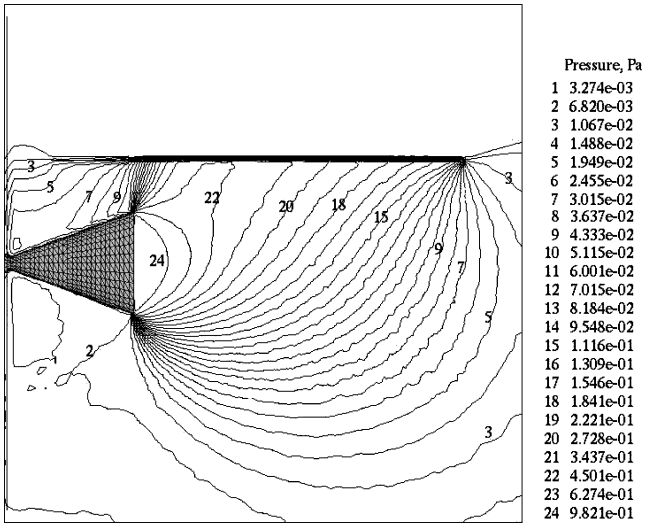

Fig. 6 Pressure field (pascals) over rough plate with triangular grooves.

about 6 mm downstream from the nozzle exit plane. The pressure values in that region are over an order of magnitude larger than those at the corresponding location in the bottom half of the plume, (i.e., part of the plume where no surface interaction exists). There is significant backflow observed as the result of the plume–surface interaction. A strong backflow will result in a contribution of backflow molecules interacting with the plenum surface to the total force. This contribution increases the total force in X direction.

The flow does not change qualitatively when a plate with a triangular surface roughness is used (Fig. 6). Quantitatively, however, the pressure maximum at the plate shifts about 1 mm downstream compared to the smooth surface case and the maximum value increases by about 10%. The pressure is generally higher for the rough plate because most of the plume molecules that collide with the surface are reflected backward in that case. This is especially noticeable in the backflow region where the pressure for the rough surface case is about two times higher. Note that the mean free path of the gas near the plate is on the order of 1 cm and is an order of magnitude larger that the roughness size. In addition to the triangular groove roughness, a rectangular groove shape has also been examined. The pressure for the latter case is somewhat lower than for the triangular one, but is still higher than for the smooth surface, as shown in Fig. 7.

The increase in the angle α of the plate measured from the plume direction from 0 to 10 deg significantly weakens the plume–surface

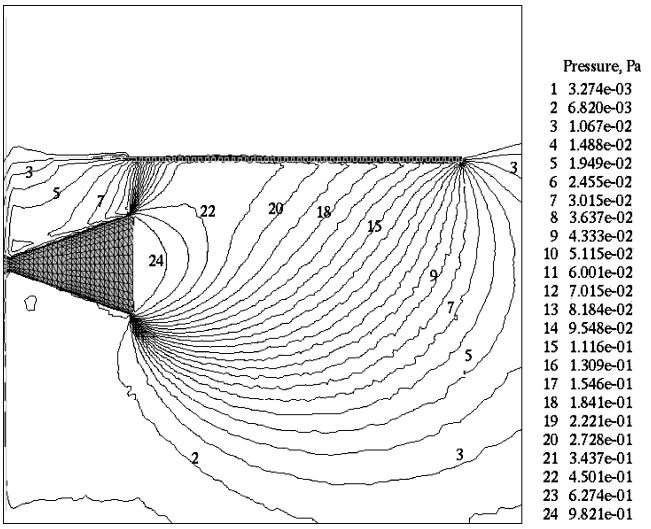

Fig. 7 Pressure field (pascals) over rough plate with rectangular grooves.

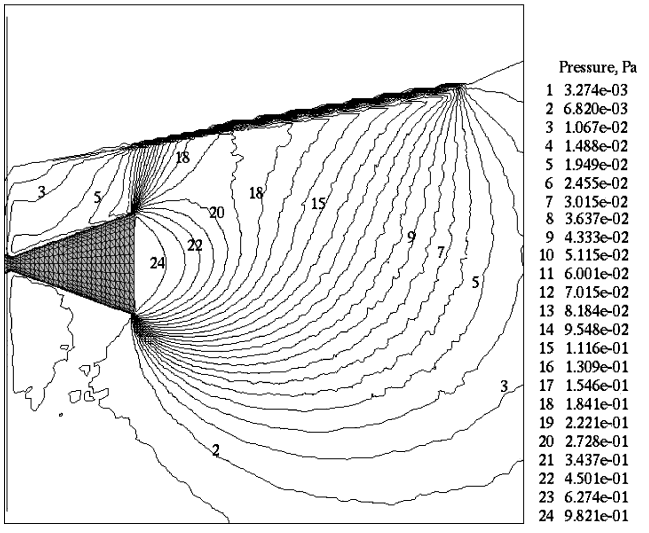

Fig. 8 Pressure field (pascals) over rough plate with triangular grooves; 10-deg plate angle.

interaction, as shown in Fig. 8. The pressure maximum is more than two times smaller for $\alpha = 10$ deg than it was for $\alpha = 0$, and the plate no longer has a noticeable effect on the flowfield in the immediate vicinity of the nozzle exit. The backflow pressure is also reduced and is only slightly higher than the corresponding pressure at the bottom-half of the plume backflow. The effect of the plate surface roughness on the pressure field for $\alpha = 10$ deg is similar to that for $\alpha = 0$ deg and is not shown here.

Consider now the effect of the surface roughness on surface forces. The distribution of the forces in the X direction (shear force) and Y direction (pressure force) over a smooth plate is shown in Figs. 9 and 10. Here, the X direction coincides with the direction of the plume, and the Y direction is perpendicular to the plate surface. The maximum of the force in the X direction, F_x, is about 0.26 N and is located close to the plate center, in the region where both molecular density and axial velocities are sufficiently large. The maximum of the force in the Y direction, F_y, is shifted a few millimeters to the nozzle exit plane, where the local gas pressure maximum is observed. The maximum F_y is about two times larger than the corresponding maximum F_x, primarily because the force from reflected molecules is finite for F_y and zero for F_x. Also, the axial velocity component of plume molecules in that region is somewhat larger than the radial one, with the incidence angle typically larger than $\alpha = 45$ deg.

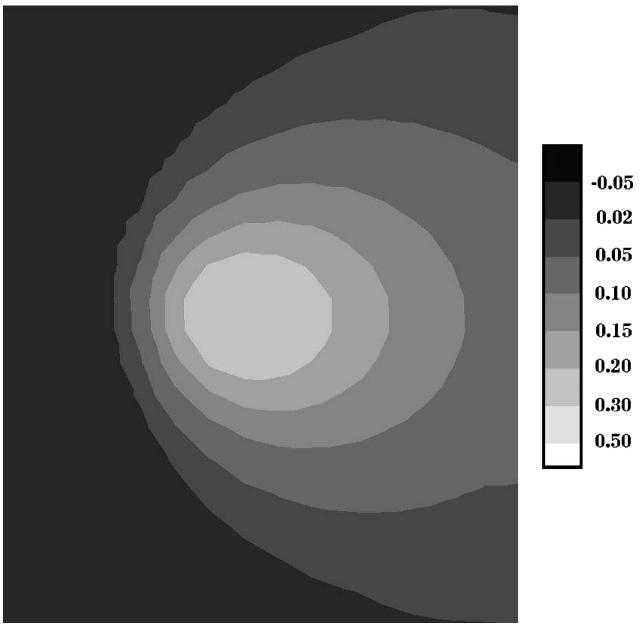

Fig. 9 Force in X direction per unit area (newtons per square meter) on a smooth plate for the 0-deg plate angle and $P_0 = 405$ Pa.

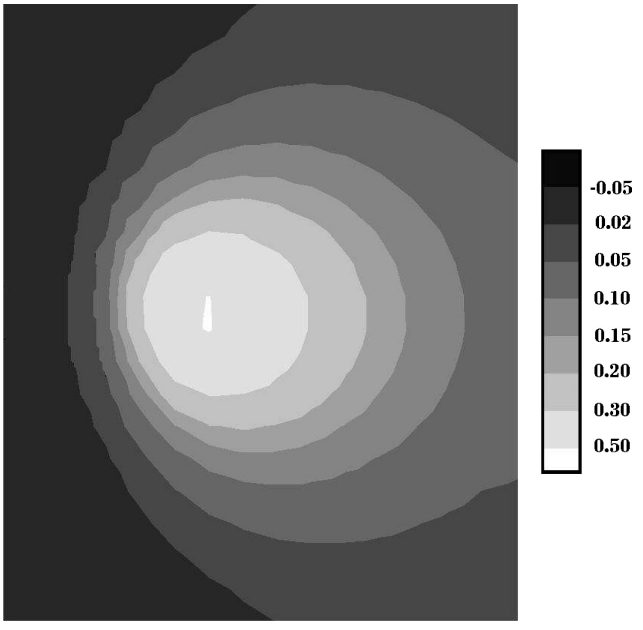

Fig. 10 Force in Y direction per unit area (newtons per square meter) on smooth plate for 0-deg plate angle and $P_0 = 405$ Pa.

Figures 11 and 12 present the corresponding force distributions for a rough surface of plate (triangular roughness). They clearly show the discontinuous structure of the force distributions. The F_x values are large on the sides of the grooves directed toward the nozzle (wind side), with the maximum value almost three times larger than the corresponding maximum on a smooth plate. The lee sides of the grooves, however, are characterized by forces that act in the direction opposite to the plume direction, therefore, reducing the large force from the wind sides. The maximum value of F_x on a rough plate is close to that of F_y. The wind–lee side structure of the surface is also clearly seen in F_y, although the direction of the forces is the same for this case.

The forces on the plate F_x and F_y and on the plenum surface F_b are presented in Table 2 for two roughness types and two angles of the plate. For the plate angle of $\alpha = 0$, the magnitude of the forces on the plate is comparable to the plume thrust force F_{th},

Table 2 Surface forces for $P_0 = 405$ Pa

Surface	Angle	F_{th}, N	$F_{x,s}$, N	$F_{y,s}$, N	F_b, N	F_{tot}, N
Smooth	0	0.309×10^{-3}	-0.6762×10^{-4}	0.1093×10^{-3}	0.1204×10^{-4}	2.5342×10^{-4}
Rectangular	0	0.309×10^{-3}	-0.7340×10^{-4}	0.1083×10^{-3}	0.1519×10^{-4}	2.5079×10^{-4}
Triangular	0	0.309×10^{-3}	-0.8256×10^{-4}	0.1124×10^{-3}	0.1808×10^{-4}	2.4452×10^{-4}
Smooth	10	0.309×10^{-3}	-0.3076×10^{-4}	0.7252×10^{-4}	0.5641×10^{-5}	2.8388×10^{-4}
Triangular	10	0.309×10^{-3}	-0.4059×10^{-4}	0.7481×10^{-4}	0.9040×10^{-5}	2.7745×10^{-4}

Table 3 Surface forces for $P_0 = 155$ Pa

Surface	Angle	F_{th}, N	$F_{x,s}$, N	$F_{y,s}$, N	F_b, N	F_{tot}, N
Smooth	0	0.949×10^{-4}	-0.2368×10^{-4}	0.3799×10^{-4}	0.4618×10^{-5}	0.7584×10^{-4}
Rectangular	0	0.949×10^{-4}	-0.2595×10^{-4}	0.3770×10^{-4}	0.6036×10^{-5}	0.7499×10^{-4}
Triangular	0	0.949×10^{-4}	-0.2960×10^{-4}	0.3822×10^{-4}	0.7315×10^{-5}	0.7262×10^{-4}

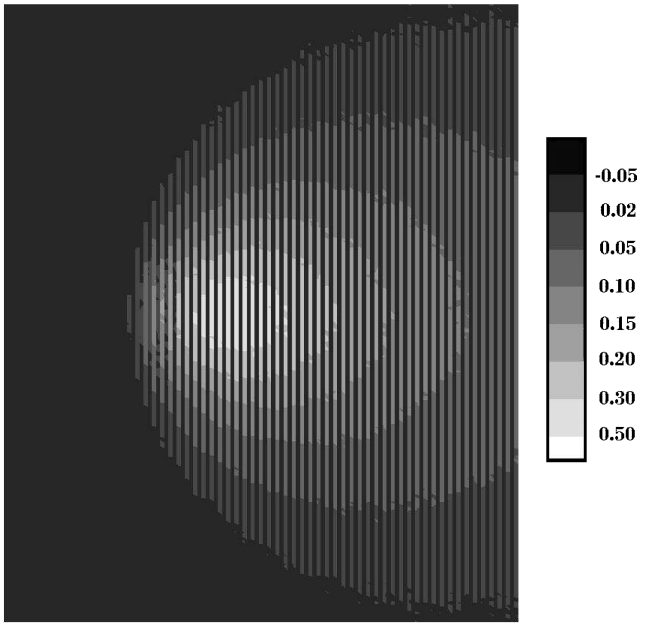

Fig. 11 Force in X direction per unit area (newtons per square meter) on rough plate for 0-deg plate angle and $P_0 = 405$ Pa.

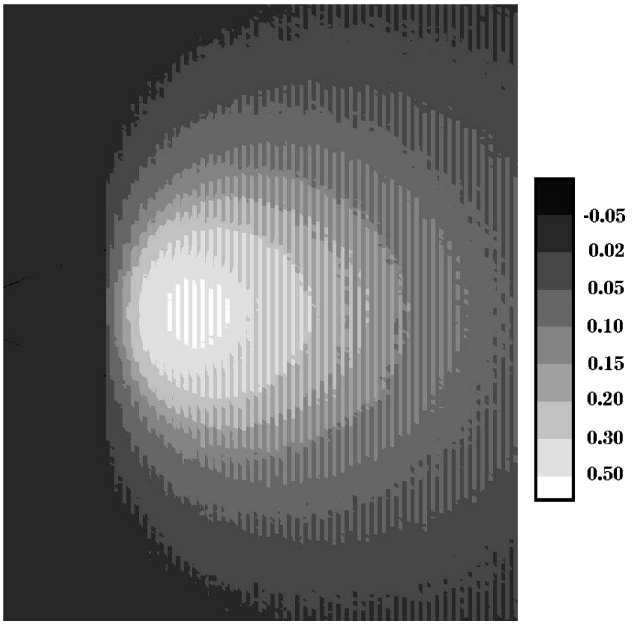

Fig. 12 Force in Y direction per unit area (newtons per square meter) on rough plate for 0-deg plate angle and $P_0 = 405$ Pa.

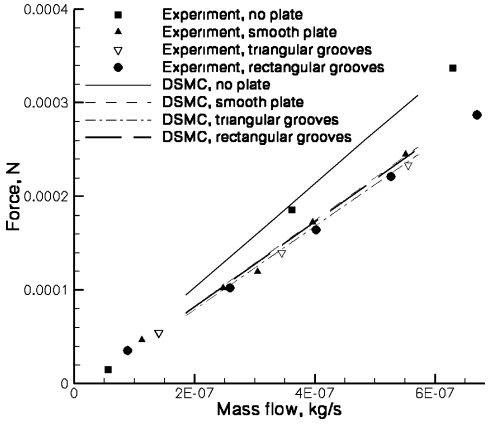

Fig. 13 Total force vs mass flow for free expansion and smooth and rough surfaces: numerical and experimental modeling.

with F_x and F_y being about 25 and 30% of the thrust, respectively. Comparison of rough and smooth surfaces shows that the magnitude of F_x is smallest for the smooth plate and largest for a plate with the triangular roughness shape. The difference is about 20% for these cases. The force in Y direction is weakly dependent on surface roughness.

Another important contributor to the total force in X direction, F_{tot}, is the force on the nozzle plenum, primarily caused by molecules reflected on the plate. This force is significantly larger for rough plates, with the value for the triangular roughness type about 50% higher than that for the smooth plate. Because the force on the plenum is in the direction opposite to that on the plate, this 50% difference considerably reduces the effect of surface roughness on F_{tot}. The difference between F_{tot} for a smooth and a rough plate with triangular grooves amounts to only about 3% of the total force. For the angle of 10 deg, this difference is only about 2.5%.

The comparison of contributions to the total force for a plume flow at $P_0 = 155$ Pa, interacting with smooth and rough surfaces, is given in Table 3. As compared to $P_0 = 405$ Pa, all forces scale approximately with the stagnation pressure, and the conclusions made for the higher pressure case are applicable for $P_0 = 155$ Pa.

VI. Interaction of Plume with a Plate: Experimental Study

Comparison of computed and measured total forces vs mass flow is presented in Fig. 13. Here, the lines that show numerical solutions were created using the values of F_{tot} listed in Tables 2 and 3, which correspond to the chamber pressures of 155 and 405 Pa. The agreement between the experimental and computed force values is good, and the difference in all cases does not go beyond a few percent. The experimental and numerical forces are within 1% for a smooth polished plate and a rough plate with triangular roughness. The values for a plate with rectangular grooves are closer to those for a smooth plate in DSMC and to a triangular grooved plate in the experiment,

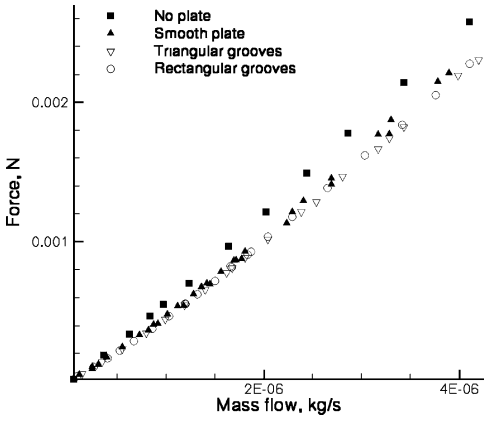

Fig. 14 Measurements of total force vs mass flow for free expansion and smooth and rough surfaces.

although the difference is rather small and may be attributed to one or several causes of experimental and numerical inaccuracies.

There are several possible sources of experimental uncertainties in this work. First, there is always a finite background gas pressure in the chamber that increases with mass flow. The background gas may impact the mass flow measurements only for plenum pressures larger than 1333 Pa, although the force (momentum flux) measurements are affected to some extent at all plenum pressures. A previous study[10] indicated that the force can be affected by less than 0.5% at the experimental conditions of this work. A thrust stand calibration of deflection angle vs applied force has been approximated to be within 3%. For a given applied force to the stand, the standard deviation of the stand's deflection was less than 1%; however, the accuracy of the calibration system must also be taken into account. Finally, there was some error associated with the manufacturing of the nozzle. The nozzle throat diameter is known only with an accuracy of 1%, and the nozzle surfaces are significantly rough. In addition to the experimental uncertainties, there are a number of numerical uncertainties. Grid resolution, maximum number of simulated molecules, effects of the subsonic boundary conditions, and gas–gas collision models all account for a numerical uncertainty estimated to be on the order of 1–2%.

The experimental results for a wider range of mass flows that correspond to plenum pressures up to about 2266 Pa are shown in Fig. 14. The addition of an engineering surface parallel to plume flow significantly reduces total force, up to 15%. The surface roughness effect is much smaller, and the effect of the roughness type is negligible. The small difference between rough and smooth surfaces is explained by the effect of the plume molecules colliding with the nozzle plenum, as discussed in the preceding section.

VII. Conclusions

Experimental and numerical modeling of a cold-gas nozzle plume interacting with engineering surfaces is performed for nitrogen propellant in the range of nozzle-throat-based Reynolds numbers from about 2 to 350. A nanonewton resolution force balance was used in the experimental study to measure thrust force of a plume expanding from a conical nozzle, and then the total force resulted from the interaction of the plume with aluminum plates attached to the same force balance. Smooth and rough plates were examined, with surface roughness introduced through a set of equally spaced 0.5-mm-wide grooves perpendicular to the flow direction.

The DSMC method was used in the numerical study, with the setup corresponding to that in the experiment. The calculated force vs mass flow was found to be in a good agreement with the corresponding experimental data. The experiments and computations showed that there is significant thrust degradation due to the plume surface interaction, with the total decrease being up to 15%. The force on the plate increases in magnitude by about 20% for the rough surface as compared to the smooth one. However, the impact of the surface roughness on total force is small, which is attributed primarily to the effect of nozzle plume molecules reflected from the plate backward to the plenum surface. The number of such molecules is significantly larger for rough surfaces.

The impact of the surface roughness inside the nozzle has been studied numerically. It was shown that the surface roughness decreases both mass flow and thrust by over 10% for Reynolds numbers on the order of one. The effect decreases with the increase of the Reynolds number and is negligible at $Re > 100$. The specific impulse is not affected by the surface roughness even at small Reynolds numbers.

Acknowledgments

This work was supported in part by the U.S. Air Force Office of Scientific Research and the Propulsion Directorate of the Air Force Research Laboratory at Edwards Air Force Base, California.

References

[1]Boyd, I., and Ketsdever, A., "Interactions Between Spacecraft and Thruster Plumes," *Journal of Spacecraft and Rockets*, Vol. 38, No. 2, 2001, p. 380.

[2]Lengrand, J.-C., Allegre, J., Bisch, D., and Skovorodko, P., "Impingement of a Simulated Rocket Exhaust Plume onto a Surface," *Rarefied Gas Dynamics, Proceedings of the 20th International Symposium*, edited by C. Shen, Bejing Univ. Press, Beijing, 1997, pp. 537–542.

[3]Ivanov, M., Markelov, G., Kaskhovsky, A., and Giordano, D., "Numerical Analysis of Thurster Plume Interaction Problems," *Proceedings of Second European Spacecraft Propulsion Conference*, ESA SP-38, 1997, pp. 603–610.

[4]Hyakutake, T., and Nishida, M., "Numerical Simulation of Rarefied Nozzle Plume Impingements," *Rarefied Gas Dynamics, Proceedings of the 22nd International Symposium*, edited by T. Bartel and M. Gallis, AIP CP 585, American Inst. of Physics, New York, 2001, pp. 806–811.

[5]Legge, H., "Plume Impingement Forces on Inclined Flat Plates," *Rarefied Gas Dynamics, Proceedings of the 17th International Symposium*, edited by A. Beylich, VCH, Aachen, Germany, 1991, pp. 955–962.

[6]Deependran, B., Sujith, R., and Kurian, J., "Impingement of Low Density Freejets on a Flat Plate," *Rarefied Gas Dynamics, Proceedings of the 20th International Symposium*, edited by C. Shen, Bejing Univ. Press, Beijing, 1997, pp. 465–466.

[7]Ketsdever, A., *Micropropulsion for Small Spacecraft*, Vol. 187, Progress Series in Astronautics and Aeronautics, edited by M. Micci and A. Ketsdever, AIAA, Reston, VA, 2000, pp. 139–166.

[8]Ketsdever, A. D., Lilly, T. C., Gimelshein, S. F., and Alexeenko, A. A., "Experimental and Numerical Study of Nozzle Plume Impingement on Spacecraft Surfaces," *24th International Symposium on Rarefied Gas Dynamics*, edited by M. Capitelli, Vol. 762, AIP Conf. Proceedings, American Inst. of Physics, Melville, NY, 2005, pp. 367–372.

[9]Jamison, A., Ketsdever, A., and Muntz, E. P., "Gas Dynamic Calibration of a Nano-Newton Thrust Stand," *Review of Scientific Instruments*, Vol. 73, No. 10, 2002, pp. 3629–3637.

[10]Ketsdever, A., "Facility Effects on Performance Measurements of Micropropulsion Systems Which Utilize Gas Expansion," *Journal of Propulsion and Power*, Vol. 18, No. 4, 2002, pp. 797–804.

[11]Rothe, D., "Electron-Beam Studies of Viscous Flow in Supersonic Nozzles," AIAA Journal, Vol. 9, No. 5, 1971, pp. 804–810.

[12]Ivanov, M., Markelov, G., Ketsdever, A., and Wadsworth, D., "Numerical Study of Cold Gas Micronozzle Flows," AIAA Paper 99-0166, Jan. 1999.

[13]Ketsdever, A. D., Clabough, M. T., Gimelshein, S. F., and Alexeenko, A. A., "Experimental and Numerical Determination of Micropropulsion Device Efficiencies at Low Reynolds Numbers," *AIAA Journal*, Vol. 43, No. 3, 2005, pp. 633–641.

[14]Ivanov, M. S., Markelov, G. N., and Gimelshein, S. F., "Statistical Simulation of Reactive Rarefied Flows: Numerical Approach and Applications," AIAA Paper 98-2669, June 1998.

I. Boyd
Associate Editor